Available online at www.sciencedirect.com

ScienceDirect

Defence Technology 10 (2014) 106–110

www.elsevier.com/locate/dt

Burning characteristics of microcellular combustible objects

Wei-tao YANG, Yu-xiang LI, San-jiu YING*

School of Chemical Engineering, Nanjing University of Science and Technology, Nanjing 210094, China

Received 22 December 2013; revised 6 March 2014; accepted 18 March 2014
Available online 2 April 2014

Abstract

Microcellular combustible objects for application of combustible case, caseless ammunition or combustible detonator-holding tubes are fabricated through one-step foaming process, in which supercritical CO_2 is used as foaming agent. The formulations consist of inert polymer binder and ultra fine RDX. For the inner porous structures of microcellular combustible objects, the cell sizes present a unimodal or bimodal distribution by adjusting the foaming conditions. Closed bomb test is to investigate the influence of both porous structure style and RDX content on burning behavior. The sample with bimodal distribution of cell sizes burns faster than that with unimodal distribution, and the concentration of RDX can influence the burning characteristics in a positive manner. In addition, the translation of laminar burning to convective burning is determined by burning rate versus pressure curves of samples at two different loading densities, and the resulting transition pressure is 30 MPa. Moreover, the samples with bigger sample size present higher burning rate, resulting in providing deeper convective depth. Dynamic vivacity of samples is also studied. The results show that the vivacity increases with RDX content and varies with inner structure.

Keywords: Microcellular combustible object; Burning characteristics; Closed bomb test

1. Introduction

Application of microcellular combustible objects containing combustible cartridge cases [1–3], caseless ammunition [4,5] and combustible detonator-holding tubes [6,7] in weapons is to save metal, ensure light weight ammunition, eliminate the disposal of spent metal case, simplify automatic firing device and add energy to propulsion system. The objects get consumed on firing and leave no smouldering or burnt residue. Traditional formulations with nitrocellulose were judged to be unsafe due to an increased sensitivity to friction, heat and static electricity [8]. Polymer bonded propellants have been used for developing the insensitive ammunition for different reasons [4]. The researchers [4,5] have employed a reaction injection moulding (RIM) process to produce the foamed thermoset PU bonded RDX propellants which present good vulnerability performance and high burning rate [5].

In our study, a new microcellular combustible object which contains a large amount of isolated cells is presented. The object based on inert polymer bonded nitramines has several superiorities, such as adjustable energy content, high burning rate, good heat and moisture resistance and low vulnerability. In addition, the cells containing gas can provide higher impact strength [9] and act as a heat insulator. The microcellular combustible objects using thermoplastic polymer as binder can be produced by a traditional solvent method and be foamed via supercritical CO_2 (SC-CO_2) as foaming agent and plasticizer. SC-CO_2 exists as a noncondensable, high-density fluid above the critical temperature (31.1 °C) and critical pressure (7.38 MPa) [10]. SC-CO_2 as both solvents and foaming agents offers many superiorities including enhanced diffusion rates [11,12], effective plasticization [13–17].

* Corresponding author.
E-mail address: sanjiuying@163.com (S.J. YING).
Peer review under responsibility of China Ordnance Society

Production and hosting by Elsevier

http://dx.doi.org/10.1016/j.dt.2014.03.003

The burning characteristics of the microcellular combustible object have been incompletely understood, and its performance contains a number of unknowns. The objective of this paper, therefore, is to study the burning characteristics and to isolate the influencing factors which affect the burning behavior in closed bomb test.

2. Experiment

2.1. Materials and manufacturing process

The basic formulation is composed of RDX and inert binder. Average particle size of fine RDX is 10 μm. The inert binder used in this study is poly methyl methacrylate (PMMA) (Altuglas® V 040). The 50 mm × 12.9 mm × 2 mm solid sheet were extruded by the solvent process and foamed via one-step foaming process [18–21]. The schematic illustration of foaming process is shown in Fig. 1. Firstly, the high pressure vessel was preheated to a desired temperature in water-bath. Then the propellant was put into the reactor. The vessel was flushed with CO_2 for a few minutes, it was pressurized to a desired pressure by a supercritical fluid equipment. The solid propellant was exposed in SC-CO_2 for a prescribed saturation time (10 h). Finally, the valve of the reactor was opened and the pressure was quenched rapidly to atmospheric pressure in 30 s, resulting in self-foaming of samples.

2.2. Sample characteristics

The morphology of sample was observed by Quanta FEG 250 scanning electron microscope (SEM). The samples were freeze-fractured in liquid nitrogen before sputter-coating with gold. The porous structures were obtained from SEM micrographs.

The burning characteristics of microcellular and solid samples were investigated by closed bomb experiments. The samples were tested in a 109 ml vessel at loading density (Δ) of 0.12 and 0.2 under the same ignition pressure (10.98 MPa). The output of CV data acquisition system was fed to computer, and maximum pressure (p_{max}) and rise time (t) were calculated. The form function of a non-porous propellant and Vieille's law were used to analyze the data of closed vessel, and the burning rates from samples which may be burning in a volumetric mode are reduced to a comparable apparent burning rate. The reduced burning rate is referred to as apparent burning rate due to the uncertainty caused by assuming a geometrical form function for microcellular propellant combustion.

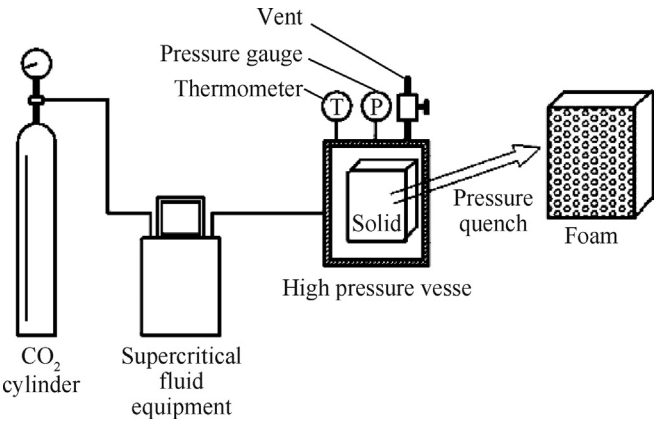

Fig. 1. Schematic illustration of foaming process in SC-CO_2.

3. Results and discussion

3.1. Inner porous structure

Fig. 2 shows the inner structures of solid and microcellular combustible objects. The microcellular samples were foamed at different conditions. Fig. 1(a) shows the inner structure of solid sample after solvent process, revealing good RDX dispersion in the binder matrix. Fig. 1(b) and (c) show that two typical porous structures with unimodal and bimodal distribution of cell sizes are obtained by adjusting the foaming condition. Sample with bimodal cell structure has a thicker porous cell wall, but the bigger inner surface resulting from microcells in matrix. Details of samples tested in closed bomb are listed in Table 1. (a). Solid sample (b) Sample with unimodal distribution of cell sizes (c) Sample with bimodal distribution of cell sizes.

3.2. Burning characteristics

Because the microcellular combustible objects contain large amounts of pores, it is believed that a convective combustion zone ahead of the flame front is responsible for the in-depth combustion or volumetric combustion phenomena. These porous energetic objects often show relatively high combustion rate in comparison to the solid one. Fig. 3 illustrates the closed bomb pressure histories for the microcellular combustible objects compared with unfoamed one. Fig. 4 shows the apparent burning rate data, reduced from the results of the closed bomb tests shown in Fig. 3.

The closed bomb histories, as shown in Fig. 3, consist of an initial pressure rose from combustion of the ignition powder, a subsequent slight pressure decrease due to heat transfer losses, and, finally, combustion of the microcellular sample. Table 2 gives the average values of total burning time, p_{30MPa}-p_{max} burning time and p_{max}. The total burning time is the time from the booster peak to the time at which p_{max} occurs and includes the sample ignition delay, and p_{30MPa}-p_{max} burning time values are defined as the time of the period from 30 MPa to p_{max}, which was supposed to a convective burning zone. It can be known from Table 2 that the combustible microcellular objects with higher RDX content show significantly shorter total burning time and p_{30MPa}-p_{max} burning time than the samples with lower RDX ratio regardless of type of inner structure. Table 2 also reveals that the samples with bimodal cell structure burn faster than that with unimodal cell structure. Compared with the solid sample, the samples with the same

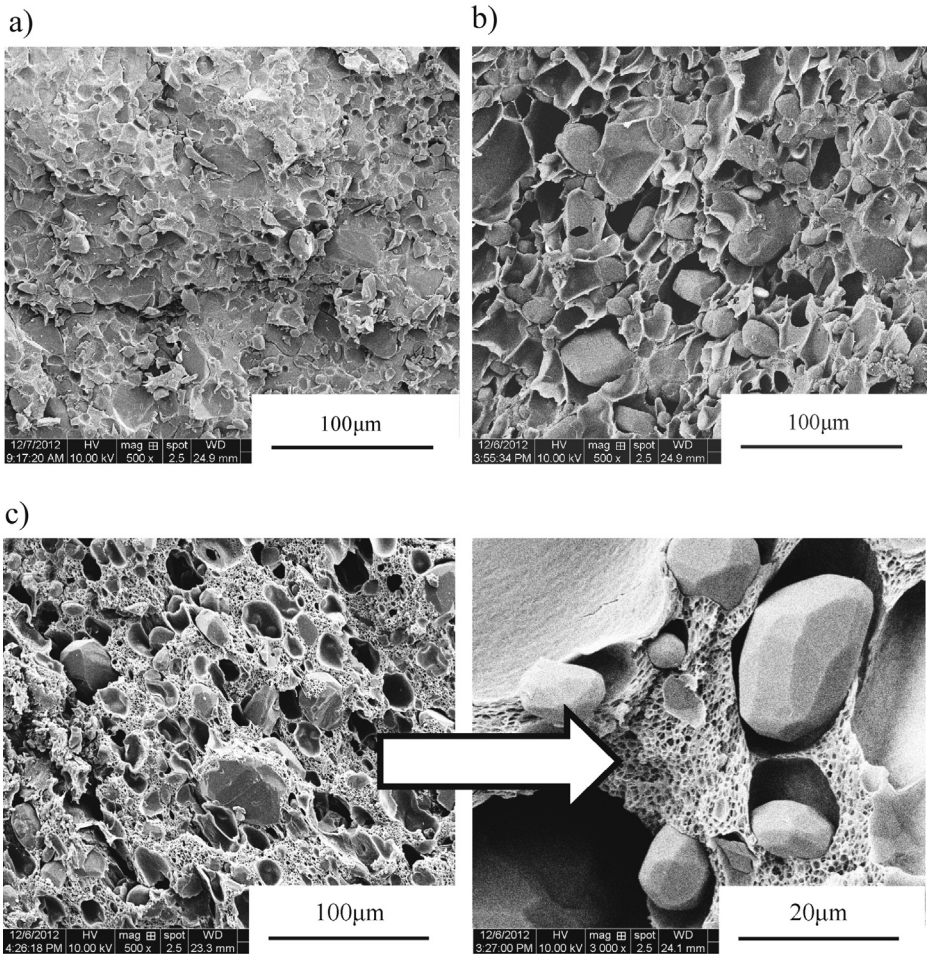

Fig. 2. Inner structures of solid and microcellular objects.

RDX content have an obviously decreased total burning time and p_{30MPa}-p_{max} burning time.

The apparent burning rates of samples are presented in Fig. 4. As shown in Fig. 4, the apparent burning rates are much bigger than unfoamed one for the giant inner surface and convective burning. The burning rate varies with the RDX content, as well as the type of porous structure. Sample 4 can burned as fast as Sample 5 which has 10% more RDX. The burning rate of sample with bimodal distribution of cell sizes is higher than that of unimodal cell structure, owing to the bigger inner surface.

Table 1
Details of samples tested in closed bomb.

Sample	[a]Formulation (weight percent)	Cell size distribution style
1	60/40	Solid
2	50/50	Unimodal
3	60/40	Unimodal
4	60/40	Bimodal
5	70/30	Unimodal

[a] RDX/polymer binder.

3.3. Transformation of laminar burning to convective burning

Although microcellular combustible objects burn convectively, combustion may originate and be sustained at the

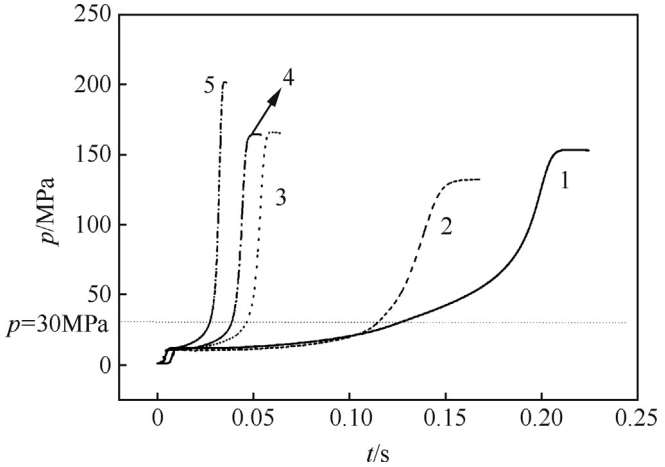

Fig. 3. Closed bomb pressure histories (loading density = 0.2).

Table 2
Results of closed bomb tests.

Sample	Total burning time/ms	p_{30MPa}-p_{max} time/ms	p_{max}/MPa
1	205.66	89.16	153.36
2	159.46	54.11	132.27
3	54.45	13.37	164.61
4	37.4490	12.377	164.41
5	29.5660	8.139	201.99

surface [8]. The burning rates of samples at two different loading densities are shown in Fig. 5. At a certain pressure ($p \approx 30$ MPa), the samples burn as non-porous propellants, and the burning rate is independent from loading density. While the pressure in chamber is high enough ($p \geq 30$ MPa) to drive hot combustion gases into the microcells in unburned zone, which in turn convectively heats to ignite the propellant. This process usually results in a ragged flame front, making the burning rate curves separated. The separation point of $p = 30$ MPa can be regarded as the transient point from laminar burning to convective burning, corresponding to the point at which pressure increased dramatically on the *p-t* curves shown in Fig. 3.

3.4. Dependence of burning rate on sample size

To further study the convective burning mechanism and the dependence of burning rate on sample size, Sample 4 was cut into smaller cuboids and tested in closed bomb. Fig. 6 shows the dependence of burning rate on the sample size. The result reveals that the samples with bigger size can reach a higher burning rate by proving deeper convective combustion depth. In addition, the burning rates of samples with bimodal cell size distribution are also identical to each other in the low pressure period until about 30 MPa, as a result of a laminar burning mechanism.

3.5. Dynamic vivacity analysis

The dynamic vivacity (L) versus B ($B = p/p_m$) curves of samples are shown in Fig. 7 and Fig. 8. It can be seen from

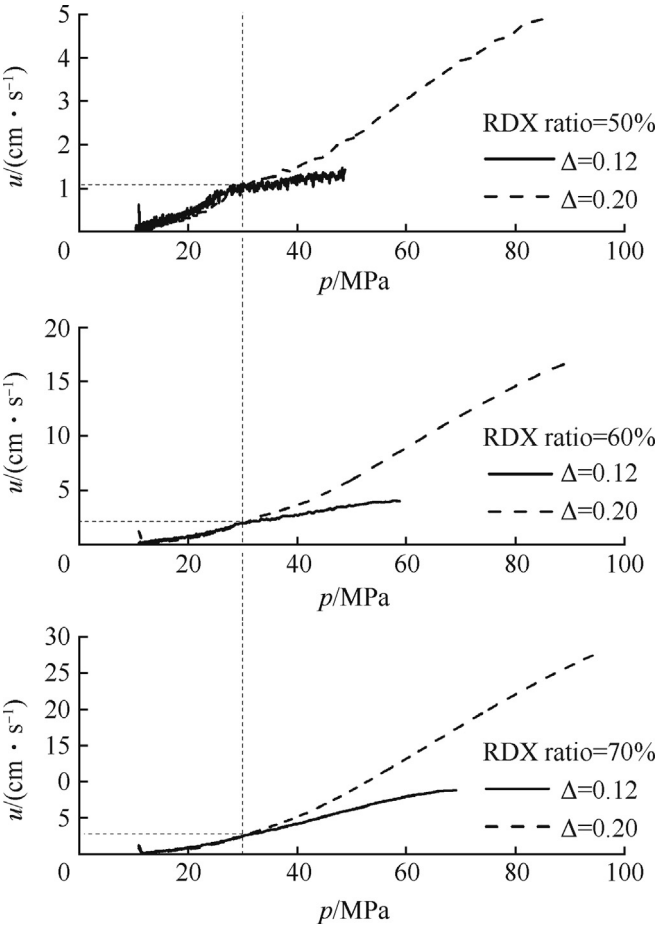

Fig. 5. Burning rate vs. pressure at different loading densities (Δ).

Fig. 7 that the vivacity of sample is influenced obviously by RDX content. The less the energetic filler (RDX) is in the formulation, the lower the dynamic vivacity is. Fig. 8 presents the dynamic vivacities of samples with constant RDX content but different inner structures (solid, unimodal and bimodal). As shown in Fig. 8, the foamed objects have bigger dynamic vivacities compared to the unfoamed ones. The L values of

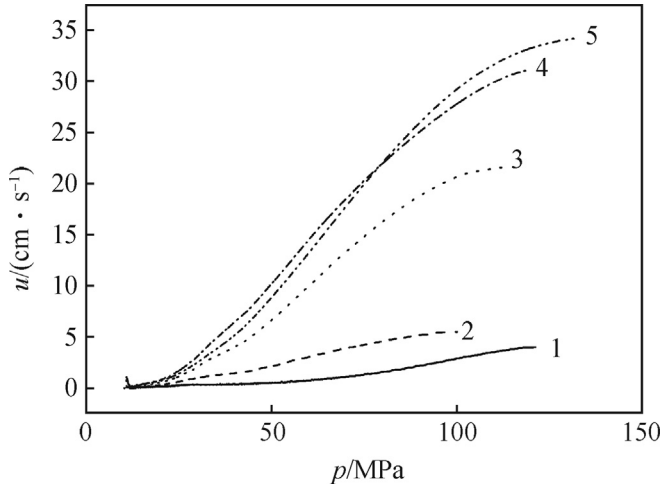

Fig. 4. Apparent burning rate vs. pressure.

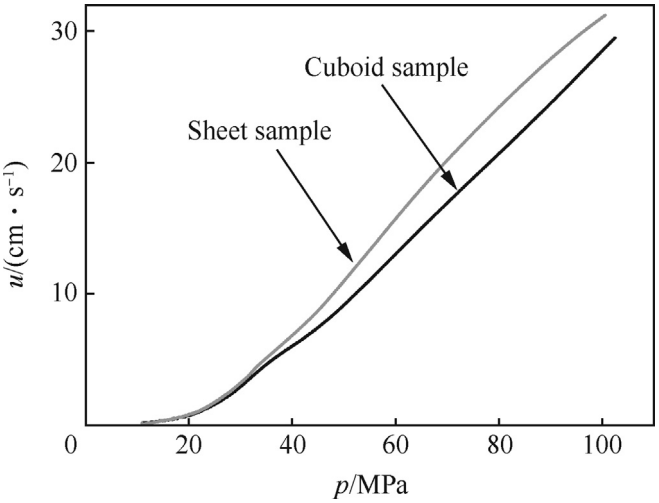

Fig. 6. $u-p$ curves of samples with different sizes.

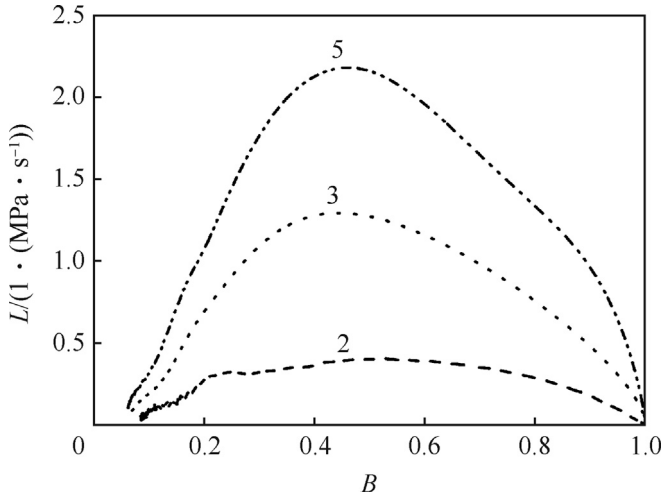

Fig. 7. Dynamic vivacities of samples as function of RDX ratio, $\Delta = 0.2$ g/cm.^{3}

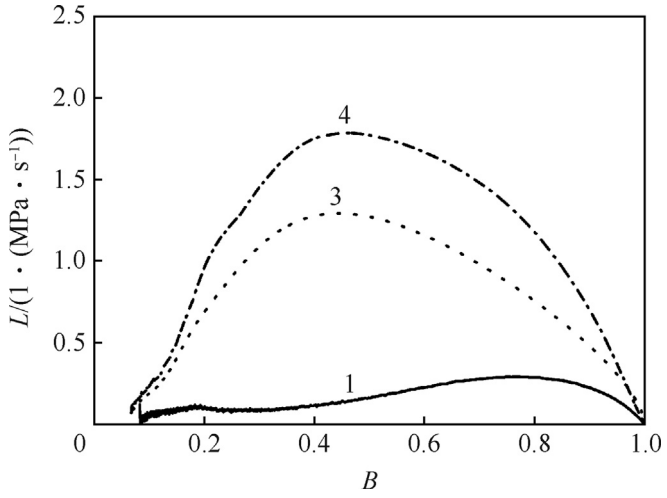

Fig. 8. Dynamic vivacities of samples with different inner structures, $\Delta = 0.2$ g/cm.^{3}

foamed samples started to decrease until $B \approx 0.5$, while for the unfoamed objects, the L values kept increasing until $B \approx 0.8$.

4. Conclusions

The burning characteristics of microcellular combustible objects in closed vessel were studied in the paper. The burning characteristics of foamed propellants can be adjusted by changing the energetic ingredients and the porous structure. Due to these manifold possibilities to adjust the specific performance profile, the microcellular combustible objects can be adapted and fine tuned for a huge variety of applications. The formulation or the inner structure of an object has to be adjusted to meet the special requirements for a concrete application.

Acknowledgments

The project was funded by the Priority Academic Program Development of Jiangsu Higher Education Institutions.

References

[1] Shedge MT, Patel CH, Tadkod SK, Murthy GD. Polyvinyl acetate resin as a binder effecting mechanical and combustion properties of combustible cartridge case formulations. Def Sci J 2008;58(3):390−7.
[2] Zimmerman FJ. Development of 7.62-mm and 38-mm combustible cartridge case ammunition. J Spacecr Rockets 1969;6(3):312−4.
[3] Zimmerman F. The development of small caliber combustible cartridge case ammunition. In: ICRPG/AIAA 3rd Solid Propulsion Conference; 1968.
[4] Böhnlein-Mauß J, Kröber H. Technology of foamed propellants. Propellants Explos Pyrotech 2009;34(3):239−44.
[5] Böhnlein-Mauß J, Eberhardt A, Fischer TS. Foamed propellants. Propellants Explos Pyrotech 2002;27(3):156−60.
[6] Zhao Y. Numerical simulation for ignition and flame-spreading of modular charge. Chin J Explos Propellants 2003;26(2):012.
[7] Ye Y, Shen R, Dai S. Comparison of fire abilities between LVD center core igniter and conventional center core igniter. Initiators Pyrotech 2001;2(87):1−4.
[8] Barnes JT, Fisher EB. Combustion mechanisms of very high burn rate (VHBR) Propellant. Phase II; 1995 [DTIC Document].
[9] Flinn B, Bordia RK, Weller J. Impact strength of high density solid-state microcellular polycarbonate foams. J Eng Mater Technol 2001;123(2):229−33.
[10] Nalawade SP, Picchioni F, Janssen L. Supercritical carbon dioxide as a green solvent for processing polymer melts: processing aspects and applications. Prog Polym Sci 2006;31(1):19−43.
[11] Tang M, Du TB, Chen YP. Sorption and diffusion of supercritical carbon dioxide in polycarbonate. J Supercrit Fluids 2004;28(2−3):207−18.
[12] Zhou C, Wang P, Li W. Fabrication of functionally graded porous polymer via supercritical CO_2 foaming. Compos Part B: Eng 2011;42(2):318−25.
[13] Alessi P, Cortesi A, Kikic I, Vecchione F. Plasticization of polymers with supercritical carbon dioxide: experimental determination of glass-transition temperatures. J Appl Polym Sci 2003;88(9):2189−93.
[14] Dong Hwang Y, Woon Cha S. The relationship between gas absorption and the glass transition temperature in a batch microcellular foaming process. Polym Test 2002;21(3):269−75.
[15] Yoon JD, Cha SW. Change of glass transition temperature of polymers containing gas. Polym Test 2001;20(3):287−93.
[16] Yu L, Liu H, Chen L. Thermal behaviors of polystyrene plasticized with compressed carbon dioxide in a sealed system. Polym Eng Sci 2009;49(9):1800−5.
[17] Handa YP, Kruus P, O'Neill M. High-pressure calorimetric study of plasticization of poly(methyl methacrylate) by methane, ethylene, and carbon dioxide. J Polym Sci Part B Polym Phys 1996;34(15):2635−9.
[18] Zhu B, Zha W, Yang J, Zhang C, Lee LJ. Layered-silicate based polystyrene nanocomposite microcellular foam using supercritical carbon dioxide as blowing agent. Polymer 2010;51(10):2177−84.
[19] Xing Z, Wu G, Huang S, Chen S, Zeng H. Preparation of microcellular cross-linked polyethylene foams by a radiation and supercritical carbon dioxide approach. J Supercrit Fluids 2008;47(2):281−9.
[20] Ito S, Matsunaga K, Tajima M, Yoshida Y. Generation of microcellular polyurethane with supercritical carbon dioxide. J Appl Polym Sci 2007;106(6):3581−6.
[21] Xu Q, Ren X, Chang Y, Wang J, Yu L. Generation of microcellular biodegradable polycaprolactone foams in supercritical carbon dioxide. J Appl Polym Sci 2004;94(2):593−7.